DEVELOPMENT OF A NOVEL HEAT-RESISTANT AUSTENITIC CAST STEEL WITH AN IMPROVED THERMAL FATIGUE RESISTANCE

B. A. Martinez Carreon and M. O. Ramos Azpeitia
Facultad de Ingeniería, Universidad Autónoma de San Luis Potosí, Dr. Manuel Nava 8, Zona Universitaria, 78290 San Luis Potosi, SLP, Mexico

J. L. Hernandez Rivera
CONACYT-Instituto de Metalurgia, Universidad Autónoma de San Luis Potosí, Sierra Leona 550, Lomas 2a Sección, 78210 San Luis Potosi, SLP, Mexico

A. Bedolla Jacuinde
Instituto de Investigación en Metalúrgia y Materiales, Universidad Michoacana de San Nicolas de Hidalgo Gral, Francisco J. Mugica S/N, Felicitas del Rio Morelia Michoacan, 58030 Morelia, Mexico

C. J. Garcia Lopez
Instituto Politécnico Nacional CIITEC-IPN, Cerrada de Cecati S/N Col Sta, Catarina, Azcapotzalco, Mexico

J. A. Ruiz Ochoa
Escuela de Ciencias de la Ingeniería y Tecnología, Universidad Autónoma de Baja California, Blvd. Universitario 1000, Unidad Valle de las Palmas, Tijuana, BC, Mexico

A. C. Gonzalez Castillo
Instituto de Metalurgia, Universidad Autónoma de San Luis Potosí, Sierra Leona 550, Lomas 2a Sección, 78210 San Luis Potosi, SLP, Mexico

https://doi.org/10.1007/s40962-022-00838-1

Abstract

In this work, the Thermo-Calc software was used to evaluate the effect of the Nb and Mn additions on the thermal phases stability for a conventional HT heat-resistant austenitic cast steel (HRACS) at high temperature. The simulations show that addition of Nb promoted the decrease in carbides (Fe, Cr)$_7C_3$ and $Cr_{23}C_6$ as well as the formation of a stable NbC at elevated temperature. Meanwhile, the Mn addition does not modify the amount of $Cr_{23}C_6$ and (Fe, Cr)$_7C_3$ and tends to reduce the (Fe, Cr)$_7C_3$ to $Cr_{23}C_6$ transformation temperature. In order to validate the thermodynamic simulations, specimens of an austenitic cast steel modified with 3.3 wt% of Nb were fabricated, characterized and compared with specimens of conventional HT steel after the application of 25, 50 and 100 continuous heating–cooling cycles in non-protected atmosphere. It was found that the Nb causes the reduction of phases that promoted the nucleation of thermal microcracks, which was in good agreement with simulations. In addition, the results indicated that Nb allowed the reduction of the number, length and propagation rate of microcracks. Therefore, this novel HRACS demonstrated to be more resistant to thermal fatigue compared to conventional HT steel in a non-protected atmosphere.

Keywords: *heat-resistant steels, thermodynamic simulation, characterization*

Received: 11 January 2022 / Accepted: 10 June 2022 /
Published online: 7 July 2022

Introduction

The conventional heat treatments which are used to increase mechanical properties of a widely number of automotive parts involve the application of severe and continuous heating and cooling cycles during the process. Most of the components and tooling used in this application are manufactured using heat-resistant austenitic cast steels,[1,2] which have high chromium and nickel content which are necessary to maintain high corrosion resistance, good creep properties and resistance to embrittlement caused by thermal shock as result of an austenitic matrix structure stabilization and fine precipitation of a complex carbide.[1–4] One of the most commonly used steels for this purpose is the heat-resistant HT steel with contents of 15–19 wt% Cr and 33–37 wt% Ni.[5] For this heat-resistant steel, the as-cast microstructure generally consists of an austenite matrix with some amounts of ferrite and the presence of interdendritic carbides.[3,6] These steels are used in the cast condition, so it is not necessary to apply any heat treatment to adjust mechanical properties. The above implies that for components and tooling manufactured with this kind of steel, the microstructure and properties will depend entirely on the chemical composition and also from the type of the casting process.

In the heat treatment industry, the application of a continuous heating and quenching cycles develops stresses that may lead to severe distortion and eventual cracking in components and tooling manufactured with HT steels, causing failures after a certain number of cycles due to thermal fatigue.[7,8] One way to increase the useful life of the components is through the modification of their microstructure by the addition of specific alloying elements. These elements can modify the microstructure of the heat-resistant steels to promote the presence of more resistant phases, which can increase the mechanical properties, corrosion and creep resistance.[4,9–11] These modifications in the microstructure can be manifested through a delay in the microcracks formation and on its growth rate decrement, which can be reflected into a higher useful life of the components and tooling.

Computational methods such as CALPHAD (calculation of phase diagrams) are employed to model thermodynamic properties for each phase and simulate multi-phase behavior in complex systems.[12,13] The basis of this method consists of describing the Gibbs energies of all phases present in an specific system by applying and fitting a mathematical model with adjustable parameters which are evaluated considering known experimental and theoretical information.[13,14] The use of software for thermodynamic calculation and kinetic simulation has become an important tool for the correct determination of chemical compositions that could lead to the development of new alloys.[12,15–17] Specifically, Thermo-Calc has been used for the optimization of the chemical composition, improvement of mechanical properties and creep resistance of certain class of HRACS, helping to accelerate their development cycle.[18–22] Because the components and tooling manufactured from these steels are employed at high temperature conditions during their whole lifetime, the thermodynamic simulation can also represent a powerful tool to study and evaluate the microstructural evolution of these steels in real conditions of service, especially at high temperature.

Although there are several classes of HRACS, the HK and HP grades[5] have been the most studied. In these alloys, it has been shown that the addition of niobium and other stronger carbide formers such as titanium and tungsten is beneficial to the solid solution hardening of the matrix and the hardening by the precipitation of carbides.[4,23–33] In particular, the NbC can be helpful for preventing propagation of microcracks and improving the thermal shock resistance of these steels because the preferential NbC crystallization decreases the volume of the $M_{23}C_6$ whose decomposition results in microcracks.[34] However, a negative aspect of this class is that they are expensive because they contain a large amount of Ni. Thus, a partial replacement of expensive Ni to inexpensive Mn, which is another strong austenite former, has been studied for the HK series with promising results.[35,36] Because of the commercial importance of the HT steel, it is crucial to investigate the role of different elements additions in their thermal fatigue behavior.

This work is part of an effort to develop new alloys based in conventional HT steel in order to enhance the lifetime of components and tools used in the heat treatment of automotive parts. Therefore, this paper presents the results of thermodynamic simulations carried out using the Thermo-Calc software to study the individual and combined effects of Nb and Mn additions on the amount and stability of the phases in the microstructure of a conventional HT steel at high temperature. The simulation results, which found the best combination in order to decrease detrimental carbides such as M_7C_3 and increase the stable NbC, were used to propose a novel chemical composition that was fabricated and then microstructurally characterized. Finally, the response of this novel alloy was evaluated and discussed with reference to a commercial HT steel in conditions of thermal fatigue.

Experimental Procedure

The thermodynamic simulations were carried using the Thermo-Calc Software and the TCFE9-Steel/Fe-Alloying v9.0 database.[37] Thermal phase stability diagrams were made for the determination and quantification of stable phases which would be present at high temperatures in this steel as function of the alloying elements addition (Nb and Mn); meanwhile, phase diagrams were calculated to determine a convenient element content. The intervals

evaluated in the simulation of both, Nb and Mn, were from 0.25 to 3.5 wt% with increments of 0.25 wt% and from 1 to 5 wt% with steps of 1 wt%, respectively. The composition that was used as the reference for the design of the new HRACS is presented in Table 1 and corresponds to a conventional HT steel.

The casting of the modified HRACS prototype was carried out in a high frequency vacuum induction furnace with a capacity of 10 kg. The vacuum melting was used in order to minimize the formation of non-metallic inclusions and minimize the oxidation of the alloying elements. HT steel ingots with the composition shown in Table 1 were used as raw material for the casting, and then, Nb was added in the form of ferroniobium particles (66.6Fe–33.3Nb) with an average size close to 5 mm. The fusion was carried out for 1.5 h at 1700 °C to ensure the homogeneity of the liquid steel. The molten steel was poured into steel permanent mold to obtain an ingot with length, width and thickness of 170, 115 and 40 mm, respectively. The mold was preheated to a temperature close to 800 °C. The chemical composition determination of the ingot was carried out using a spectrophotometer Spectromax-8 LMX06.

The microstructural characterization was made on specimens obtained from the modified HRACS and from a conventional HT steel for comparison purposes. The microstructural characterization was performed using an optical microscope (OM) Olympus GX51 and a scanning electron microscope (SEM) JEOL 6610LV. For both techniques, the samples were metallographically prepared using successive stages of grinding with SiC sandpapers and polishing with diamond paste of 6, 3 and 1 μm as abrasives, until obtaining a mirror-type finish surface. Prior to characterization, the samples were etched with the Marble's reagent (5g $CuSO_4$ + 25 mL HCl + 25 mL Water). Electrochemical extraction was done in modified HRACS in order to demonstrate the nature of carbides. The extraction was done by using a solution of 10 mL of HCl in 90 mL of ethanol and applying a current density of 0.08 A/cm^2 and 2 V for 40 h. A sample with dimensions of 12 × 12 × 30mm was employed in the cell. After this time enough powder was produced for X-ray diffraction analysis. The conditions for XRD were: a scanning interval of 30–90°, a step size of 0.2 and 2°/min in scanning speed.

The cast ingot from both steels was cut into smaller pieces of the following dimensions: 10 × 10 × 50 mm. The metallic pieces, after metallography preparation carried out as described above, were subjected to 25, 50 and 100 continuous heating–cooling cycles in non-protected atmosphere using an electric resistance box furnace. Each thermal cycle consisted in heating at 1000 °C for 60 min followed by a water quenching to room temperature. To evaluate the thermal fatigue damage, an average of the length and number of all internal surface cracks observed in specimens after a metallographic preparation were estimated in the pieces from conventional HT and modified HRACS steel subjected the mentioned thermal cycles by using optical microscopy. The average number of cracks and their average length were obtained from 30 fields, each field with a magnification of 5 × and an area of 5.91 mm^2, resulting in a total measurement area of 168 mm^2. In other experiments, cylindrical compression samples were subjected to the same sequence of thermal cycling for both steels, and then, they were tested by compression according to ASTM E9 in a Shimadzu universal testing machine AG100 with a capacity of 100 kN using a crosshead speed of 1 mm/min. The determination of the YS was made in samples in initial cast condition and after the corresponding thermal cycling.

Results and Discussion

Thermodynamic Analysis of Reference Alloy

The conventional HT steel was selected as the reference alloy for the design of a new one with improved thermal fatigue resistance. Figure 1 shows the phases that would be present in the microstructure at thermodynamic equilibrium conditions as a function of temperature for a conventional HT steel with the chemical composition showed in Table 1. Since alloying elements are insufficiently diffused between solid phases, these thermal phase stability diagrams are not directly applicable for as the cast structures of this kind of alloys which tend to solidify under non-equilibrium conditions; however, they represent a powerful tool to study these alloys in real conditions of service at high temperature. As can be seen in Figure 1, at high temperature, it is expected that the whole matrix will correspond to austenite phase rich in Ni–Cr together with the chromium-iron carbide with (Fe, Cr)$_7$C$_3$ stoichiometry

Table 1. Nominal Chemical Composition of a Conventional HT Steel

Element	C	Ni	Cr	Si	Mo	Mn	Nb	W	Fe
Composition (wt%)	0.55	35	17	1.25	0.25	1	0.01	0.01	Bal.

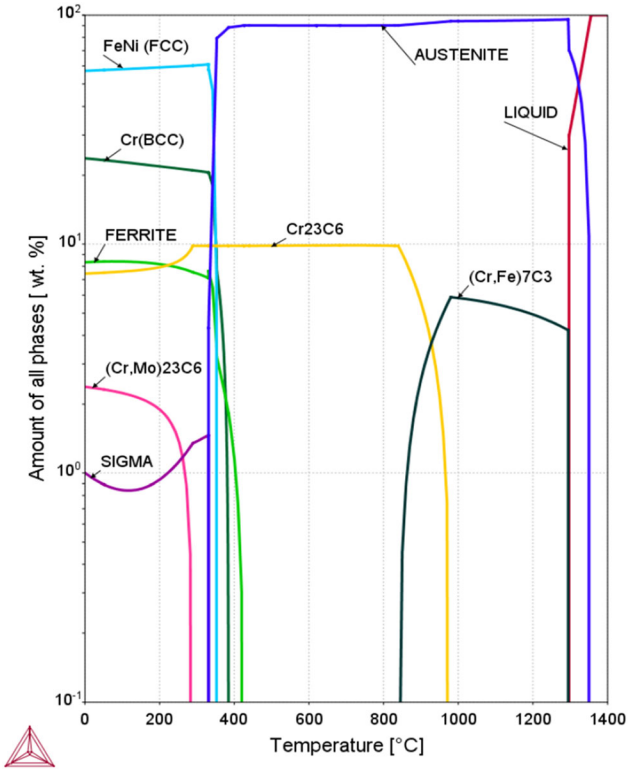

Figure 1. Thermal phase stability diagram obtained by thermodynamic simulation using the Thermo-Calc software, which show the phases as a function of temperature in a conventional HT steel with the chemical composition showed in Table 1.

which in equilibrium conditions (as thermal cycling is applied), it begins its transformation to chromium carbide with $M_{23}C_6$ stoichiometry.

Its import to note that the interval of temperature where the (Fe, Cr)$_7C_3$ to $Cr_{23}C_6$ transformation occurs, corresponded to the typical temperature range for the quenching of automotive parts, and therefore, it plays a critical role in the microstructural degradation by thermal fatigue in components and tooling manufactured with these HT steels. Specifically, it has been reported that micro-cracks that occur by the thermal shock in HRACS are caused by primary (Fe, Cr)$_7C_3$, which was detected in as-cast state.[34] It has been reported that in some HRACS at high temperature, the transformation of the primary M_7C_3 carbides into the stable $M_{23}C_6$ carbide could be accompanied by the precipitation of a very fine secondary carbide with the same stoichiometry ($M_{23}C_6$), which depending of parameters such as volume fraction and spatial distribution, can improve the creep resistance.[38]

Thermodynamic Composition Design: Effect of Nb Addition

The effect of adding Nb in different amounts on the conventional chemical composition of HT steel can be seen in Figure 2a–c, which show the stable phases when Nb is added in 0.5, 2.0 and 3.5 wt%, respectively.

The main effect at high temperature of the 0.5 wt% of Nb addition is the presence of 0.55 wt% of the niobium carbide (NbC), which is stable up to 620 °C. Another effect observed is the modification of the amounts of (Fe, Cr)$_7C_3$ and $M_{23}C_6$ carbides, for example, at 950 °C the amount of (Fe,Cr)$_7C_3$ decreases from 3.5 to 2.5 wt%; meanwhile, for the carbide $M_{23}C_6$, it increases from 3.0 to 4.5 wt%. These changes of the phases stability in equilibrium conditions, promoted by Nb addition, have also been reported in other types of HRACS such as HP.[26,27]

Thermodynamic Simulation: Effect of Mn Addition

As mentioned above, Ni is added to high-temperature resistant steels to improve resistance to thermal fatigue, and however, it is one of the elements which increase the price of steel. On the other hand, Mn which also stabilizes the austenite has been used as a partial substitute for Ni in order to reduce costs.[6,35,36] Therefore, the following group of simulations was carried out with the aim of reducing the alloying costs of the new HRACS by substituting Ni with Mn. The simulation corresponding to additions of the order of 5 wt% of Mn is shown in Figure 3a.

Comparing with the initial HT steel simulation presented in Figure 1, it can be noted that the addition until 5 wt% of Mn has not a significant effect on the amount of (Fe, Cr)$_7C_3$ and $Cr_{23}C_6$ carbides at high temperature. This last finding agrees well with experimental data which shows that the volume fraction of total carbides (M_7C_3 and MC) in commercial high Ni austenitic cast steels is very similar, when Ni is replaced with 2.0–20 wt% of Mn.[35,36] Finally, Figure 3b shows the distribution of Mn in all phases as a function of temperature. It can be observed that at high temperature, practically, all Mn is in solid solution within the austenitic matrix, and only around of 0.3 wt% Mn contributes to the partial substitution of Cr in $Cr_{23}C_6$ carbide. For the present investigation, it was only considered in this modeling a partial replacement up to 5 wt% of Mn because the role of Mn as an austenite promoter decreases when the Mn content exceeds 6.0 wt%,[40] in addition for large content of this element, the volume fraction of M_7C_3 carbide and the possibility to form ferrite phase at high temperature (close to 800 °C) increases.[35,36]

Thermodynamic Simulation: Effect of Simultaneous Nb and Mn Additions

In the present work, the individual analysis of the Nb and Mn addition from the thermodynamic simulations showed both advantages and disadvantages in the stability of the

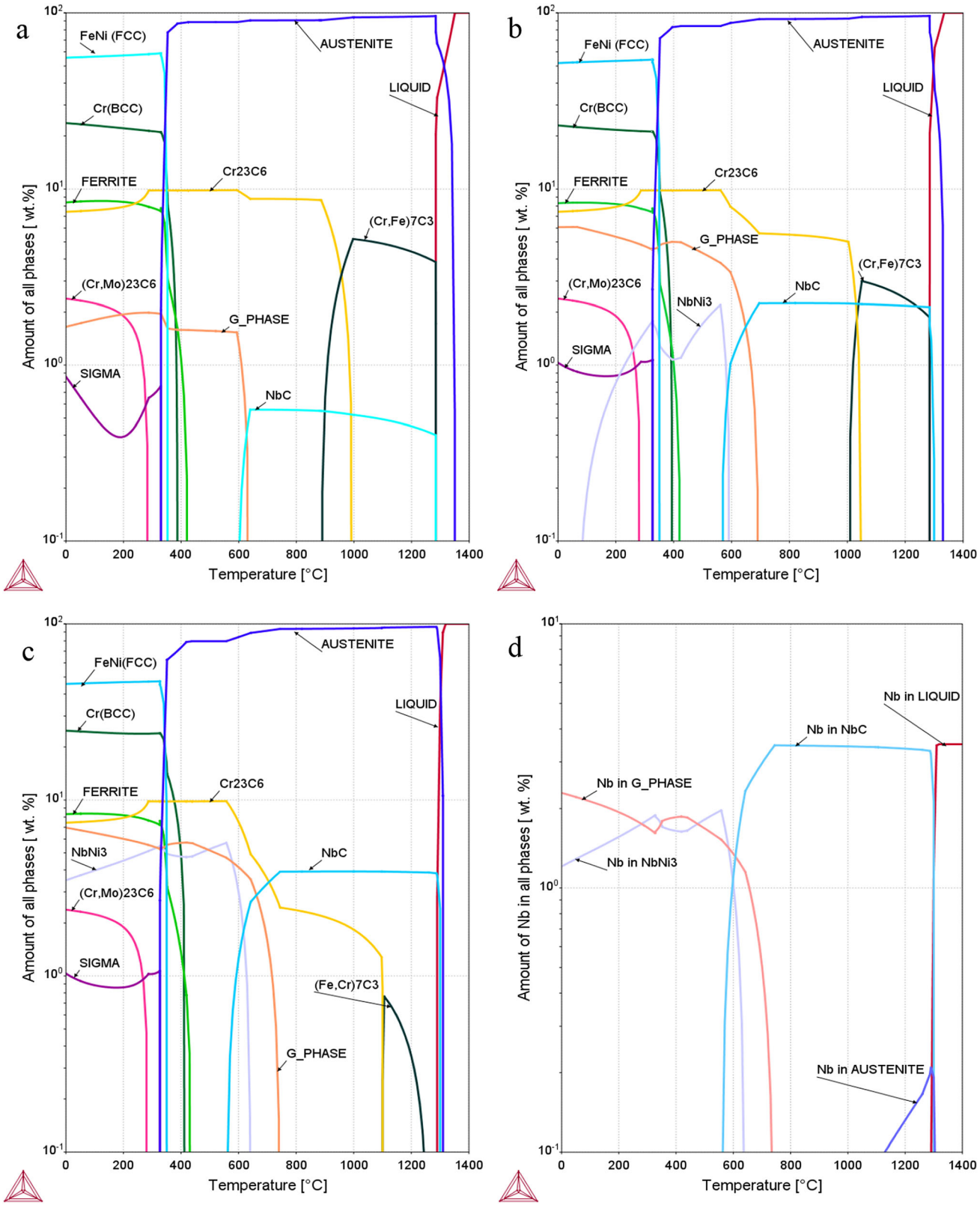

Figure 2. Thermal phase stability diagrams obtained by thermodynamic simulation using the Thermo-Calc software, which show the phases as a function of temperature in a HT steel with the chemical composition showed in Table 1 with Nb addition of: (a) 0.5 wt%, (b) 2 wt%, (c) 3.5 wt% and (d) distribution diagram of the 3.5 wt% Nb in all phases.

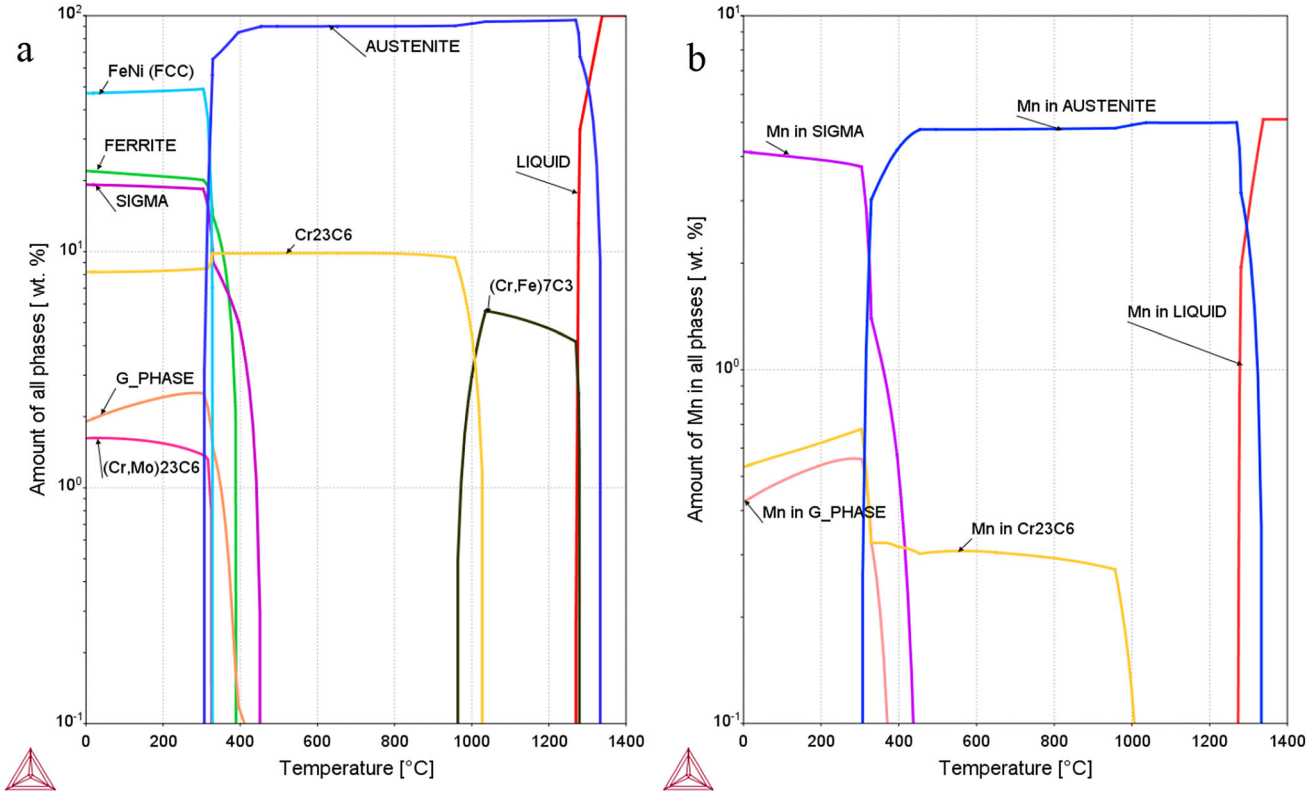

Figure 3. (a) Thermal phase stability diagram obtained by thermodynamic simulation using the Thermo-Calc software, which shows the phases as a function of temperature in a HT steel with the chemical composition showed in Table 1 with addition of 5 wt% Mn. (b) Distribution diagram of the 5wt% Mn in all phases.

phases present in the steel at high temperature. Based on this analysis, simulations were performed to assess the combined effect of the addition of Nb and Mn. Figure 4 shows the effect of a proposed modification of the chemical composition of HT steel, which consisted of a reduction of Ni from 35 to 30 wt% with the corresponding increment of 5 wt% Mn and the addition of Nb up to 3.5 wt%. It can be seen in Figure 4, that at high temperature, the behavior of carbides NbC, (Cr, Fe)$_7$C$_3$ and Cr$_{23}$C$_6$ is similar to that described in Figure 2c; however, the amount of (Cr,Fe)$_7$C$_3$ is smaller and it is stable up to 1150 °C.

The development process of a new HRACS with an improved thermal fatigue resistance includes the presence of a high-strength austenitic matrix and the dispersion of NbC precipitates; at the same time, it is important the minimization of the Cr-rich carbides.[18] Therefore, the composition of a new prototype should be designed to achieve these specific microstructural criteria; in addition, it must be considered the service requirements such as heat treatment temperatures and number of cycles. Based on the thermodynamic simulation results, it is clear that at high temperature, the options where the Nb content is around 3.5 wt% without and with contents of Mn close to 5 wt% are attractive in order to achieve the microstructural characteristics mentioned above. Therefore, it was decided for a first prototype, to modify the chemical composition of a conventional HT type steel with only 3.3 wt% of Nb in order to increase the stable NbC; meanwhile, the second prototype will be investigated in a further work. For the first prototype, carbon content was fixed in 0.6 wt% considering that high carbon content is beneficial in order to decrease the crack growth in similar austenitic cast steel,[41] and the content of Si was fixed in 0.9 wt% to ensure the fluidity of metal during pouring. The proposed chemical composition for the new HRACS and the experimental chemical composition determined from the fabricated prototype are shown in Table 2, and the corresponding thermal phase stability diagram is presented in Figure 5. In this last figure, it can be seen, that at high temperature (from 800 to 1000 °C), the stablity of carbides NbC, (Cr, Fe)$_7$C$_3$ and Cr$_{23}$C$_6$ is similar to that described in Figures 2c and 4, so these results will be taken as a reference during the characterization of the microstructure developed in the cast steel after thermal cycling.

Microstructural Characterization of HRACS Prototype

Figure 6 shows the micrographs for both, a conventional HT and for the prototype of a new HRACS in as-cast condition. The microstructure of a conventional HT steel at low magnifications (Figure 6a) exhibits a dendritic

microstructure with an austenitic matrix and semi-continuous network of eutectic carbides at the dendritic boundaries, as has been reported in similar alloys.[11,35,36,38,42] At higher magnifications (Figure 6b), it can be seen that there are carbides distributed in the interdendritic spaces and in some regions present an irregular lamellar morphology, which is in agreement with previous observations for these alloys.[38,43] This second phase of the eutectic could be (Fe, $Cr)_7C_3$ type which was predicted in the thermodynamic simulation of Figure 1. Figure 6c corresponds to as-cast microstructure of the new HRACS prototype at low magnifications, and it exhibits a more refined dendritic microstructure with an austenitic matrix and phases present both, at the dendritic boundaries and inside the dendrites. At higher magnifications (Figure 6d), it can be seen that these phases, which could be eutectic carbide (Cr, $Fe)_7C_3$, present laminar morphologies. These features agreed well with the ones reported in similar steels where the content of elements such as Ti and Nb was increased.[11,44]

The comparison of Figure 6a and c is clear that the addition of niobium has promoted fragmentation of the as-cast microstructure. The dendritic arm space (DAS) measures for both conditions showed a value of 66.5 μm for conventional HT and 27 μm for the HRACS prototype. Since the cell boundary areas expand as the DAS decreases, carbides become more homogeneously distributed. In similar alloys, this microstructural feature has been correlated with a high temperature properties improve and consequently with a retardation in the initiation and propagation of microcracks.[34] In Figure 6d, equiaxed polygonal particles are observed dispersed homogenously in the

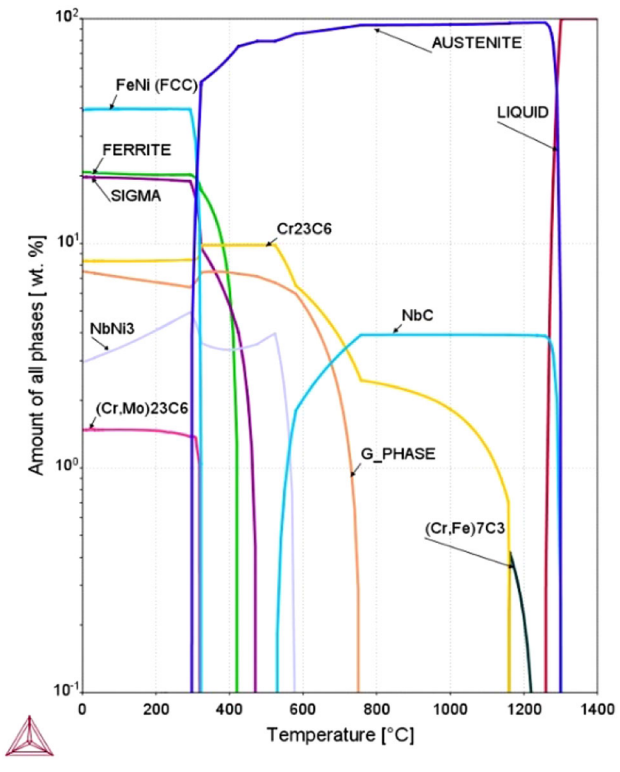

Figure 4. Thermal phase stability diagram obtained by thermodynamic simulation by using the Thermo-Calc software, which shows the phases as a function of temperature in a HT steel with the chemical composition showed in Table 1 with additions of 5wt% of Mn and 3.5 wt% of Nb.

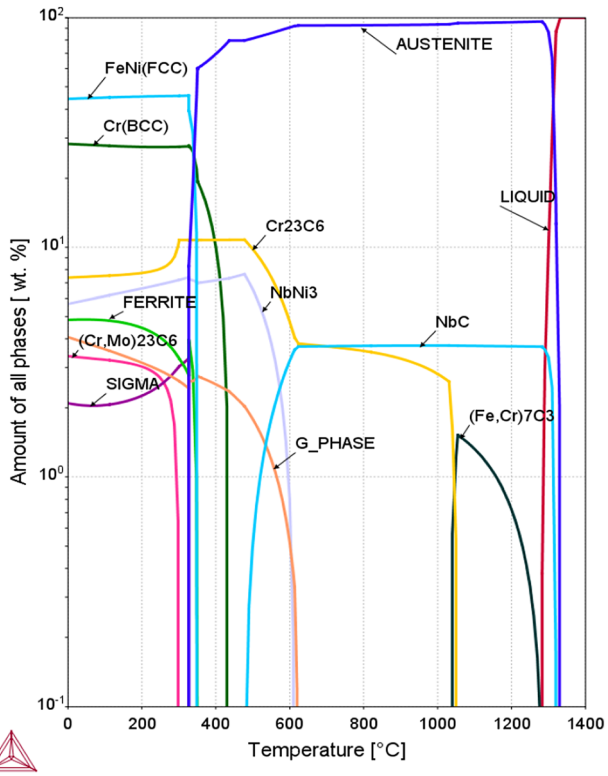

Figure 5. Thermal phasestability diagram obtained bythermodynamic simulationusing the Thermo-Calc soft-ware, which show the phases asa function of temper-ature in aHT steel with the proposedchemical composition shown in Table 2.

Table 2. Proposed and Experimental Chemical Composition for Casting Prototype of the New HRACS

Element	C	Ni	Cr	Si	Mo	Mn	Nb	W	Fe
Proposed chemical composition (%wt)	0.60	33.0	15.0	0.90	0.35	1.0	3.30	0.03	Bal.
Experimental chemical composition (%wt)	0.63	32.32	14.61	0.91	0.36	0.91	3.27	0.03	Bal.

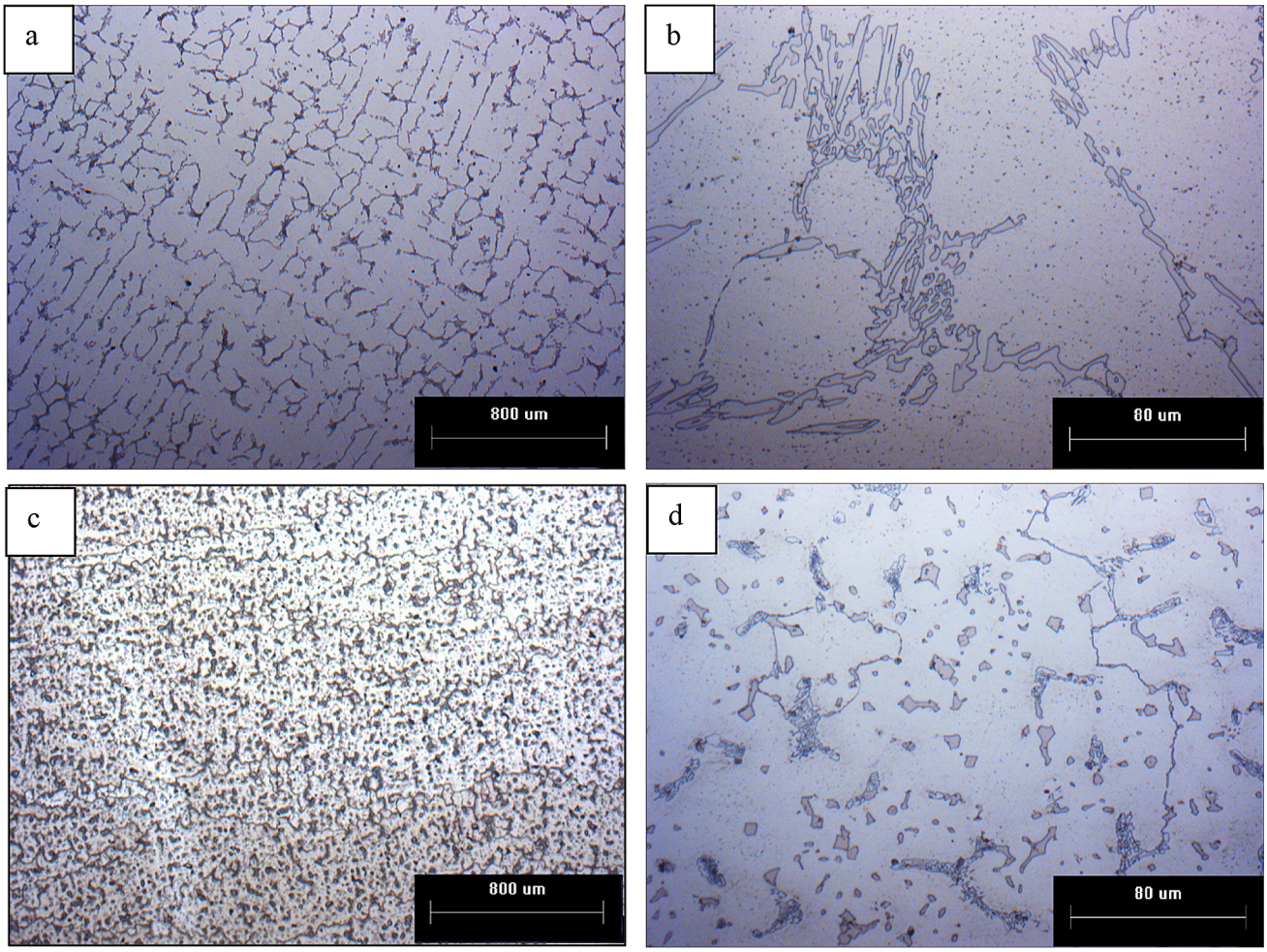

Figure 6. Optical micrographs showing the microstructure at different magnifications of: (a, b) Conventional HT austenitic cast steel; (c, d) new prototype of the HRACS.

matrix, which could be presumably NbC, since stabilizing elements such as Nb reduce the solubility of carbon in austenite and tend to form this type of carbide.[44,45]

The micrographs obtained by SEM for conventional HT steel and for the HRACS prototype are shown in Figure 7. In conventional HT steel, carbides were localized in boundaries of the dendritic microstructure (Figure 7a) and presented elongated and faceted morphology (Figure 7b). For the new prototype similar primary carbides also were detected in the interdendritic boundaries but with a minor size and with irregular form (Figure 7c, d). Additionally, in this last sample, another carbides randomly arranged within the matrix (white particles in Figure 7c and d) with polygonal morphology were observed. These findings, which are consistent with the observed by optical microscopy, are in agreement with the reported in similar cast austenitic steels with large additions of Nb.[11,20,39]

Carbides in both microstructures were identified by SEM-EDS and X-ray diffraction (XRD). In conventional HT steel, eutectic carbide observed in Figure 7b was identified as $(Cr, Fe)_7C_3$; meanwhile, in the new HRACS, the presence of the same fragmented carbide $(Cr, Fe)_7C_3$ (Figure 8c) and NbC carbide with octahedral morphology (Figure 8d) was confirmed by the XRD and the SEM-EDS analysis obtained from the extracted HRACS powder. It is important to note that for conventional HT steel and for the new HRACS, G, σ and ferrite phases were not observed in the samples, and also, no diffraction peaks of the same phases were detected which agrees with a previous report.[34] This is because the thermodynamic equilibrium could not be achieved completely during the casting cooling, and therefore, phases predicted by the thermodynamic simulations at room temperature may be not present. Specifically, the lack of ferrite in microstructure is important because a low weight fraction of primary δ-ferrite has been associated with an improving of low cycle fatigue performance in cast alloys.[46]

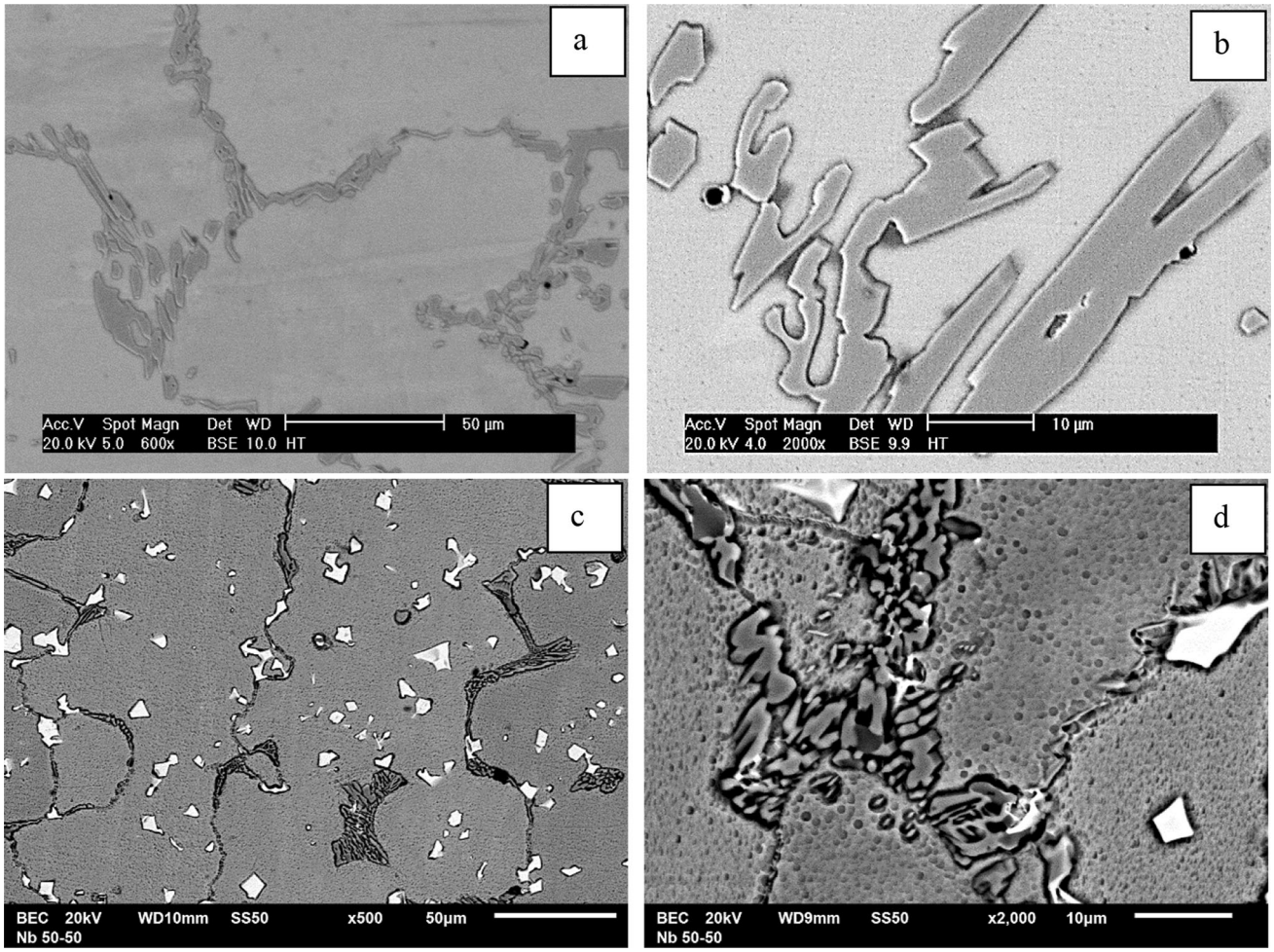

Figure 7. SEM micrographs showing the microstructure at low (500 ×) and high (2000 ×) magnifications of: (a, b) Conventional HT austenitic cast steel; (c, d) New prototype of the HRACS.

Fatigue Thermal Damage Evaluation of HRACS Prototype

The main reason which limits the life of components and tooling working under high temperature conditions during heat treatment processes is their cracking as consequence of thermal stresses originated by temperature gradients, in particular, the level of damage is increased under continuous heating–cooling conditions (thermal fatigue).[7,9] In other investigations, it has been demonstrated that the addition of Nb in the HRACS promoted the formation of a stable NbC, which helped to delay the development of the microcracks, resulting in an improvement of the thermal shock resistance for this alloy grade.[34,39] In order to evaluate if the chemical modification proposed in this work could help to improve the thermal fatigue of conventional HT austenitic steel, a quantification and size evaluation of internal microcracks were carried out in samples with 25, 50 and 100 thermal cycles for both steels. In Figure 9, it can be observed some optical micrographs used for this evaluation.

From the comparison between Figure 9a and b, it can be seen that for 25 cycles, the conventional HT steel presents larger intergranular microcracks that are very close to each other, compared to new HRACS, where the microcracks are smaller and the distance between them is greater. For 50 cycles, it is observed in Figure 9c that the cracks continued to propagate until they coalesced in conventional HT steel, resulting in an increase in their size compared to HRACS modified with Nb (Figure 9d). It can be seen that after 100 cycles, the microcracks in the conventional HT steel continued to grow longitudinally and also transversely (Figure 9e), likewise in the steel modified with Nb (Figure 9f), where it is observed that the microcracks continued growing and began to coalesce. The dark contrast features around the microcracks observed in Figure 9e were detected as oxides by SEM-EDS analysis. In general, the steel modified with Nb exhibited a smaller microcrack length size in all aforementioned conditions, which indicates that the Nb addition was effective to reduce the amount of thermal fatigue cracking, since both steels were subjected to the same testing conditions. In both steels, after the application of thermal cycles, the $(Fe, Cr)_7C_3$ and

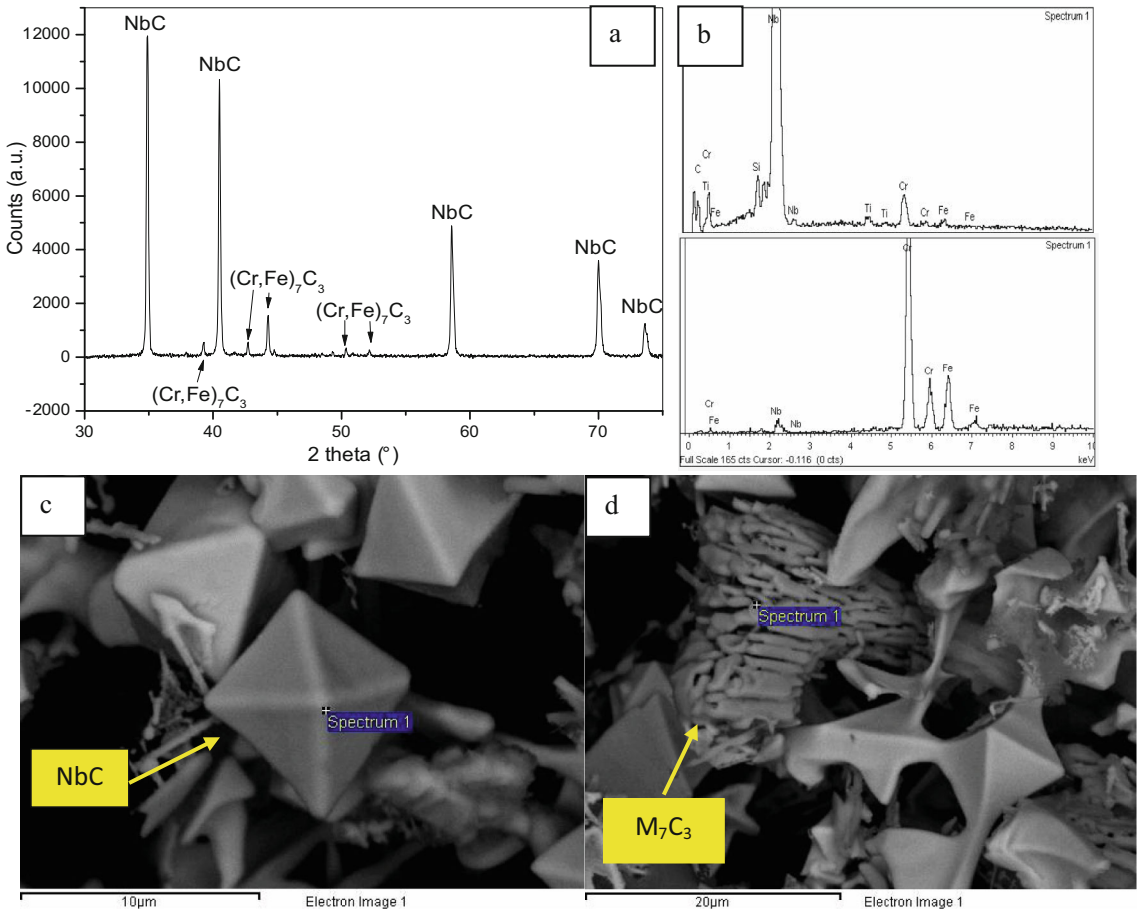

Figure 8. (a) XRD diffractogram from extracted powders from HRACS sample, (b) SEM-EDS diagrams, (c and d) SEM micrographs showing the NbC and M_7C_3 carbides, respectively.

$M_{23}C_6$ carbides were principally observed in the vicinity of microcracks. The presence of this last carbide is expected from the transformation of the (Fe, Cr)$_7C_3$ to $M_{23}C_6$ as a consequence of the heat exposure during the thermal cycling and confirms previous observations in similar heat-resistant alloys evaluated after prolonged times at high service temperatures.[24,28,34] A deeper analysis of the carbides transformation role after thermal continuous cycles is currently being carried out. The results obtained from this analysis will be reported in a future manuscript.

The results of the quantification and length size evaluation of internal microcracks by image analysis for both steels are presented in Figure 10. It is important to remark that the principal effect of the Nb addition was the reduction in the amount and average length of the microcracks observed as function of the thermal cycles number. Specifically after applied 25 cycles to conventional HT steel, were detected 201 microcracks with an average length size of 323.3 µm, meanwhile for the Nb modified HRACS with the same cycles number, 32 microcracks with an average length size 120.6 µm were observed. For 50 thermal cycles, an increment of twofold in the amount and length of microcracks for both steels was observed.

In conventional HT steel, the decrease observed in the microcracks quantity after 50 thermal cycles is due to a coalescence phenomenon; meanwhile, in the modified austenitic steel with Nb, the number of microcracks continued to grow, which could mean that this phenomenon had not yet occurred. Finally, in the HT steel with 100 thermal cycles, 82 microcracks with an average length of 952 µm were found; meanwhile, for the new austenitic cast steel, only 70 microcracks with an average length of 695 µm were recorded. The results show that the application of heating–cooling cycles leads to an increase in the average length of internal microcracks in both steels, which are associated with microstructural changes like the precipitation or transformation of carbides. However, the modified austenitic steel with Nb showed lower values for all cases (a decrease from 25% to 37% compared to conventional steel). Although the microcracks number also increased with the cycles, it is clear that this number was lower in the Nb-modified steel, in particular up to 50 cycles, where the decrement was approximately 85%.

The above results are comparable with those which reported a favorable effect in the thermal shock resistance in similar austenitic heat-resistant alloy by the additions of

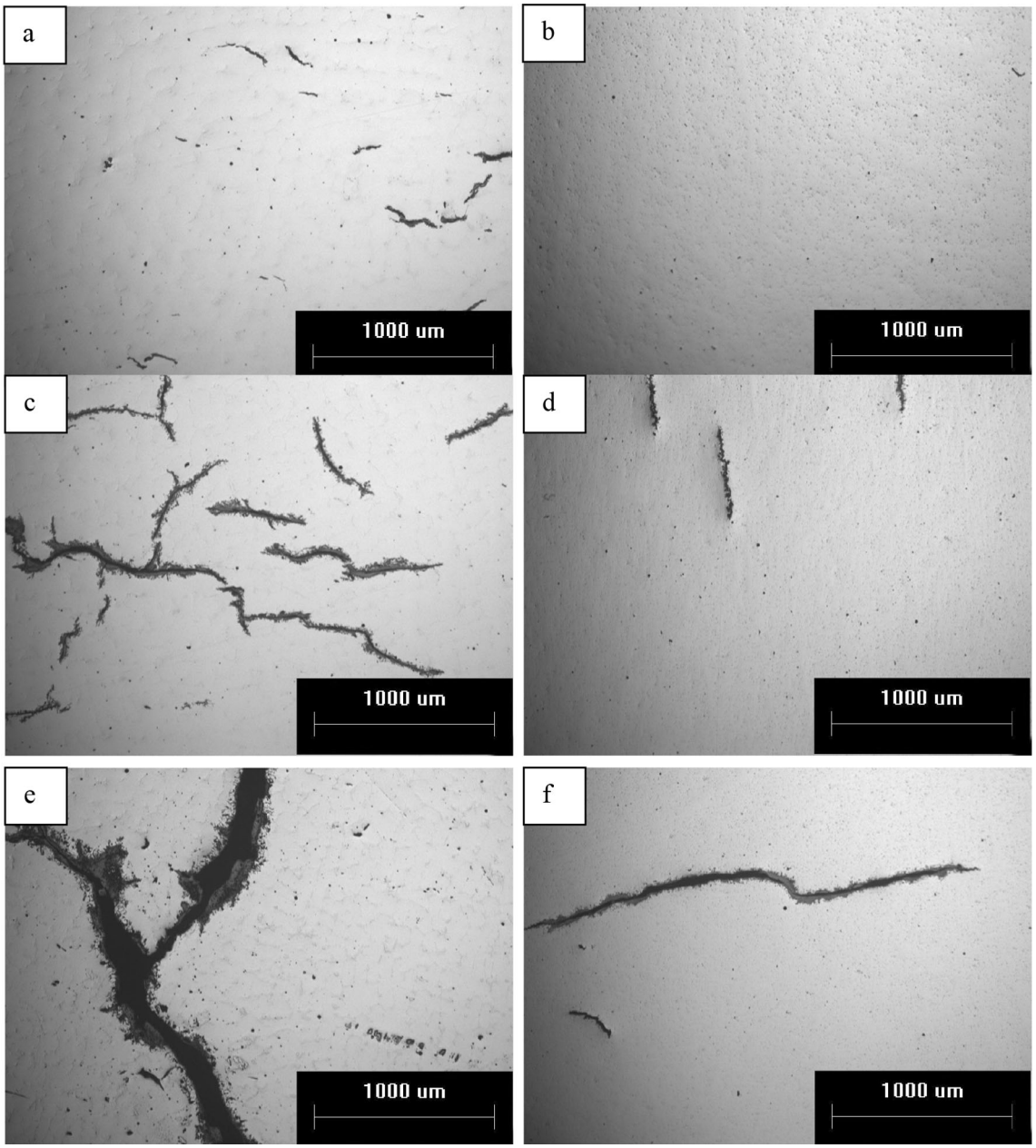

Figure 9. Optical micrographs showing the damage by thermal fatigue cracks as function of heating–cooling cycles in conventional HT austenitic cast steel (a, c, e) and in new prototype of the cast austenitic cast steel (b, d, f). 25 cycles (a, b), 50 cycles (c, d) and 100 cycles (e, f)

1.25 wt% Nb after 300 cycles of thermal shock test.[34] Under the conditions of cyclic changes of temperatures, the main source of microstresses is the foremost textural stresses formed as the result of differences in the values of the coefficient of thermal expansion α between the carbides and the austenitic matrix.[9] In this work, it was carried out an initial estimation of the Nb addition effect on the α using a previous expression obtained by linear regression analysis,[39] resulting in values of $\alpha = 18.97 \times 10^{-6}$1/K and $\alpha = 18.38 \times 10^{-6}$1/K for a conventional HT and modified HRACS, respectively. This estimation suggests that the Nb addition helped to decrease the value of α and this agrees with experimental values in HP alloy where the addition of 3.0 wt% of Nb decreased the α value from 17.9×10^{-6} to 17.75×10^{-6}1/K.[39]

Finally, Figure 11 shows the yield strength values obtained from the compression test as a function of thermal cycles for the conventional HT steel and the HRACS. The yield stress value in HT steel increases from 202 MPa in the cast condition to 368 MPa with 100 thermal cycles. It is important to mention that, in the as-cast condition, the yield stress of HRACS modified with Nb is 48 MPa that is greater than conventional HT steel and with 25 thermal cycles, it presents a yield stress of 300 MPa, which tend to stabilize up to 100 cycles. The continuous hardening of the

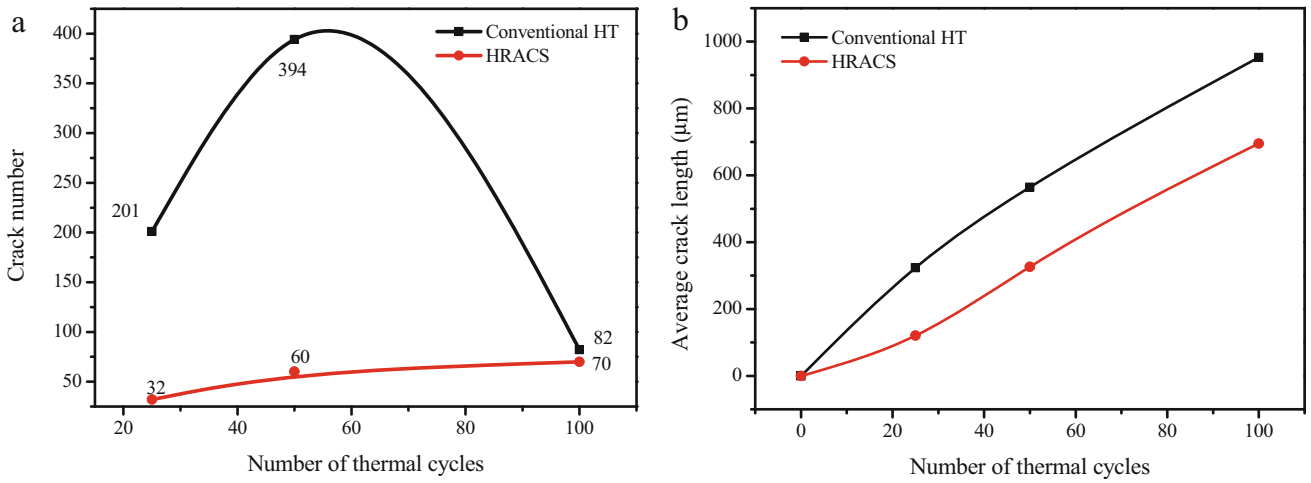

Figure 10. Evaluation of the internal microcracks in samples from the conventional HT steel and from the new prototype of HRACS as function of the thermal cycles. (a) Microcracks number; (b) average length of microcracks.

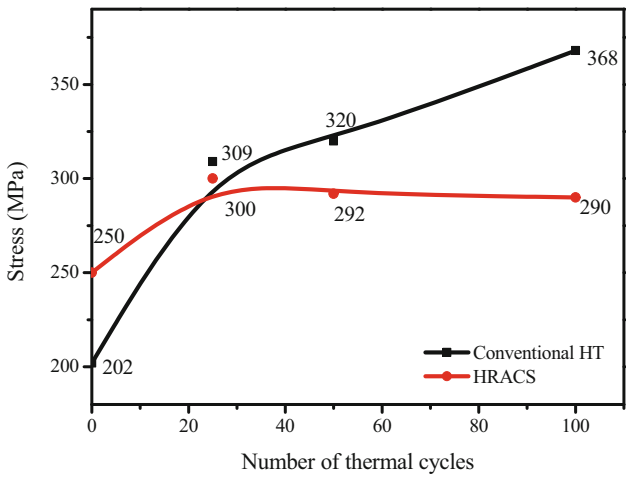

Figure 11. Values of yield strength obtained from compression tests carried out in samples of conventional HT steel and the HRACS as function of thermal cycles.

conventional HT steel that is evidenced in Figure 11 could be a consequence of the microstructural changes as has been reported in similar alloys with longer time exposures at high temperatures;[39] these changes include transformation of primary M_7C_3 carbides into $M_{23}C_6$ carbides, precipitation of a fine secondary $Cr_{23}C_6$ and the fomation of other phases (G and Z for example) as has been predicted in the simulation results presented in "Thermodynamic Analysis of Reference Alloy" section.

From results of the present investigation, it can be suggested that the damage decrement in the thermal fatigue in HRACS can be related to the reduction of phases that promote the nucleation of thermal cracks, like $(Fe, Cr)_7C_3$ or $Cr_{23}C_6$ carbides, and the increment of stable phases, which improve mechanical resistance at high temperature, like the NbC. However, deeper analyses by transmission electron microscopy (TEM) of the microstructural evolution as function of the thermal cycles in both steels are needed in order to correlate the role of the quantity, nature and size of precipitates in the thermal fatigue resistance of the new HRACS.

Conclusions

From the analysis of the results obtained in this work, the following can be concluded.

(1) Thermodynamic simulations showed that at equilibrium, individual additions of Nb close to 3.5 wt% in a conventional HT austenitic steel, encouraged the formation of the stable NbC promoting at the same time a considerable decrement of Cr_7C_3 carbide and modifying their corresponding temperature of transformation toward $Cr_{23}C_6$ carbide from 950 to 1100 °C.

(2) Thermodynamic simulations showed that in equilibrium, individual additions up to 5 wt% of Mn did not modify the amount of $Cr_{23}C_6$ and Cr_7C_3 carbides with respect to a conventional HT austenitic steel. Meanwhile, simultaneous additions of 5 wt% Mn and 3.5 wt% Nb promoted amounts of the NbC, $(Cr, Fe)_7C_3$ and $Cr_{23}C_6$ carbides at high temperature, similar to those obtained with individual large additions of Nb. Therefore, a proposal with the individual addition of Nb was selected as first viable option to development a new HRACS.

(3) The microstructural characterization of a new HRACS modified with 3.3 wt% of Nb showed that, in cast condition, the addition of Nb diminished the dendritic arm spacing from 66.5 to 27 μm and promoted the formation of stable NbC carbide with an octahedral morphology dispersed throughout the austenitic matrix, instead of the eutectic Cr_7C_3 carbide, which

tended to decrease in comparison with a conventional HT. Therefore, the NbC formation partially suppressed the formation of carbide Cr_7C_3 as was predicted by the thermodynamic simulation.

(4) The addition of 3.3 wt% of Nb in a conventional HT steel promoted changes in the microstructure which enhanced the reduction of the number and average length size of cracks after continuous heating–cooling cycles in non-protected atmospheres. It was suggested that the increment observed in the thermal fatigue resistance was a direct consequence of the Cr_7C_3 and $Cr_{23}C_6$ carbides inhibition in conjunction with the precipitation of the NbC in the new HRACS.

Acknowledgments

The authors are grateful for the financial support granted through project 511-6/17-7930 of the program support for the incorporation of NPTC, as well as the facilities granted by the Materials Engineering Training Center of the UASLP (CCIM-UASLP), by the Materials Institute at Universidad Michoacana de San Nicolas de Hidalgo and by the Metallurgy Institute of the UASLP to carry out this work. Also, the authors appreciate the technical support from Abraham Gonzalez Lara for the electrochemical tests for extraction of the carbides.

REFERENCES

1. A. Drotlew, M. Garbiak, B. Piekarski, Cast steels for creep-resistant parts used in heat treatment plants. Arch. Foundry Eng. **12**, 31–38 (2012)
2. B. Piekarski, A. Drotlew, Cast functional accessories for heat treatment furnaces. Arch. Foundry Eng. **10**, 183–190 (2010)
3. M. Blair, T.L. Stevens, *Steel casting handbook*, 6th edn. (ASM International, Novelty, 1995), pp. 2–17
4. R. Voicu, J. Lacaze, E. Andrieu, D. Poquillon, J. Furtado, Creep and tensile behaviour of austenitic Fe–Cr–Ni stainless steels. Mater. Sci. Eng. A **510–511**, 185–189 (2011)
5. ASTM A297, Standard specification for steel castings, Iron-Chromium and Iron-Chromium-Nickel, heat resistant, for General Application. 1–3 (2003)
6. J. Van der Geer, J.A.J. Hanraads, R.A. Lupton, Heat and corrosion resistant castings: their engineering properties and applications. Nickel Development Institute Publication. **266**, 1–52 (2000)
7. J Tuleja, Fracture formation in austenitic cast steel during thermal fatigue. Arch. Foundry Eng. l8, 139–142 (2008)
8. A.D. Gianfrancesco, *Materials for ultra-supercritical and advanced ultra-supercritical power plants*, 1st edn. (Elsevier, Amsterdam, 2017), pp. 99–119
9. B. Piekarski, The thermal fatigue behaviour of creep-resistant Ni–Cr cast steel. Arch. Foundry Eng. **7**, 155–158 (2007)
10. S. Jung, C. Jeon, Y. Hee Jo, W.M. Choi, B.J. Lee, Y.J. Oh, S. Jang, S. Lee, Effects of tungsten and molybdenum on high-temperature tensile properties of five heat-resistant austenitic stainless steels. Mater. Sci. Eng. A **656**, 190–199 (2016)
11. B. Piekarski, Effect of Nb and Ti additions on microstructure and identification of precipitates in stabilized Ni–Cr cast austenitic steels. Mater. Charact. **47**(3–4), 181–186 (2001)
12. A.A. Luo, Material design and development: from classical thermodynamics to CALPHAD and ICME approaches. Calphad **50**, 6–22 (2015)
13. N. Saunders, A.P. Miodownik, *CALPHAD (calculation of phase diagrams): a comprehensive guide*, 1st edn. (Elseiver, Amsterdam, 1998), pp. 1–6
14. H.L. Lukas, S.G. Fries, B. Sundman, *Computational thermodynamics: the Calphad method*, 1st edn. (Cambridge University Press, Cambridge, 2007), pp. 1–3
15. U.E. Klotz, C. Solenthaler, P.J. Uggowitzer, Martensitic–austenitic 9–12% Cr steels—alloy design, microstructural stability and mechanical properties. Mater. Sci. Eng. A **476**, 186–194 (2008)
16. S.C. Cha, S.H. Hong, I. Kim, M.Y. Kim, J.Y. Suh, J.H. Shim, W.S. Jung, J. Park, CALPHAD-based alloy design for advanced automotive steels—Part I: development of bearing steels with enhanced strength and optimized microstructure. Comput. Coupling Phase Diagr. Thermochem. **54**, 165–171 (2016)
17. S.C. Cha, S.H. Hong, M.Y. Kim, J. Park, J.H. Shim, W.S. Jung, M. Rath, E. Kozeschnik, CALPHAD-based alloy design for advanced automotive steels—Part II: compositional and microstructural modification for advanced carburizing steels. Comput. Coupling Phase Diagr. Thermochem. **54**, 172–180 (2016)
18. B.C. Schaffernak, H.H. Cerjak, Design of improved heat resistant materials by use of computational thermodynamics. Calphad **25**(2), 241–251 (2001)
19. Y.H. Zhang, M. Li, L.A. Godlewski, J.W. Zindel, Q. Feng, Effective design of new austenitic cast steels for ultra-high temperature automotive exhaust components through combined CALPHAD and experimental approaches. Mater. Sci. Eng. A **683**, 195–206 (2017)
20. Y. Zhang, J. Yang, CALPHAD-based alloy design of cast austenitic heat-resistant steels with enhanced strength at 1000 °C. Comput. Coupling Phase Diagr. Thermochem. **67**, 01–11 (2019)
21. K. Tanaka, H. Kawaura, N. Matsumoto, K. Nishino, Alloy design of a cost-effective and castable heat-resistant iron alloy. Comput. Coupling Phase Diagr. Thermochem. **30**, 415–420 (2006)
22. D. Rojas, J. Garcia, O. Prat, G. Sauthoff, A.R. Kaysser-Pyzalla, 9%Cr heat resistant steels: alloy

design, microstructure evolution and creep response at 650 °C. Mater. Sci. Eng., A **528**, 5164–5176 (2011)
23. Q.Z. Chen, C.W. Thomas, D.M. Knowles, Characterization of $20Cr_{32}Ni_1Nb$ alloys in As-cast and ex-service conditions by SEM, TEM and EDX. Mater. Sci. Eng. A **374**, 398–408 (2004)
24. F. Tancret, J. Laigo, F. Christien, R. Le Gall, J. Furtado, Phase transformations in Fe–Ni–Cr heat-resistant alloys for reformer tube applications. Mater. Sci. Technol. **34**(11), 1–11 (2018)
25. E.A. Kenik, P.J. Maziasz, R.W. Swindeman, J. Cervenka, D. May, Structure and phase stability in a cast modified-HP austenite after long-term ageing. Scripta Mater. **49**, 117–122 (2003)
26. G.D. De Almeida, L.H. De Almeida, T.L. Da Silveira, I. Le May, Niobium additions in HP heat-resistant cast stainless steels. Mater. Charact. **29**, 387–396 (1992)
27. A.R. Andrade, C. Bolfarini, L.A.M. Ferreira, A.A.A. Vilar, C.D. Souza Filho, L.H.C. Bonazzi, Influence of niobium addition on the high temperature mechanical properties of a centrifugally cast HP alloy. Mater. Sci. Eng. A **628**, 176–180 (2015)
28. M. Mostafaei, M. Shamamnian, A. Saatchi, H. Purmohamed, M. Amini, S.M. Mir, A. Tirana, J. Ezadi, Effect of aging temperature on structural evolution of HP-Nb heat resistant steel. Int. J. ISSI **6**(1), 30–33 (2009)
29. R. Voicu, E. Andrieu, D. Poquillon, J. Furtado, J. Lacaze, Microstructure evolution of HP40-Nb alloys during aging under air at 1000 °C. Mater. Charact. **60**(9), 1020–1027 (2009)
30. J. Guo, C. Cheng, H. Li, J. Zhao, Min, J. Guo, C. Cheng, H. Li, J. Zhao, Min, Microstructural analysis of $Cr_{35}Ni_{45}Nb$ heat-resistant steel after a five-year service in pyrolysis furnace. Eng. Fail. Anal. **79**, 625–633 (2017)
31. M. Attarian, A. Karimi-Taheri, S. Jalilvand, A. Habibi, Microstructural and failure analysis of welded primary reformer furnace tube made of HP-Nb micro alloyed heat resistant steel. Eng. Fail. Anal. **68**, 32–51 (2016)
32. M. Attarian, A. Karimi-Taheri, Microstructural evolution in creep aged of directionally solidified heat resistant HP-Nb steel alloyed with tungsten and nitrogen. Mater. Sci. Eng. A **659**, 104–118 (2016)
33. A.R. Andrade, C. Bolfarini, L.A.M. Ferreira, C.D. Souza Filho, L.H.C. Bonazzi, Titanium micro addition in a centrifugally cast HPNb alloy: high temperature mechanical properties. Mater. Sci. Eng. A **636**, 48–52 (2015)
34. T. Okuyama, T. Higashizono, N. Huynh, K. Luan, M. Kudo, Effect of Nb on thermal-shock resistance of austenitic heat resistant cast steel. Mater. Trans. **61**(9), 1711–1716 (2020)
35. S. Jung, Y. Hee Jo, C. Jeon, W.M. Choi, B.J. Lee, Y.J. Oh, G.Y. Kim, S. Jang, S. Lee, Replacement of Ni by Mn in high-Ni containing austenitic cast steels used for turbo-charger application. Metall. and Mater. Trans. A. **48A**, 568–574 (2017)
36. J. Yoo, W.M. Choi, B.J. Lee, G.Y. Kim, H. Kim, W.D. Choi, Y.J. Oh, S. Lee, Replacement of Ni by Mn in commercial high-Ni austenitic cast steels used for high performance turbocharger housings. Metall. and Mater. Trans. A. **50A**, 2585–2593 (2019)
37. TCFE9-Steel/Fe-Alloying, The Thermo-Calc Steels Database, upgrade by B.J. Lee, B. Sundman at KTH, Stockholm (1999)
38. M. Roussel, Sauvage, M. Perez, D. Magne, A. Heat, A. Steckmeyer, M. Vermont, T. Chaise, M. Couvrat, Influence of solidification induced composition gradients on carbide precipitation in FeNiCr heat resistant steels. Materialia **4**, 331–339 (2018)
39. Ueta S, Hamano S, Noda T, Okabe M, Abe N. Development of Thermal Fatigue Resistant Austenitic Cast Alloys for High Temperature Engine Exhaust Gas Systems. SAE Technical Paper. 2003; 1–10
40. Pistorius PC, Toit M, Low Nickel Austenitic Stainless Steels: Metallurgical Constraints. Proceedings Twelfth International Ferroalloys Congress Sustainable Future, Finland Helsinki, 2010; 911–18
41. S.J. Zhu, Y. Wang, S.G. Xu, F.G. Wang, Influence of carbon on creep crack growth of a cast HP alloy. Mater. Sci. Eng. A **127**, L7-10 (1990)
42. R. Tuttle, Thermal analysis study of heterogeneous nuclei in stainless steels. Inter. J. Metalcast. **6**, 27–34 (2012). https://doi.org/10.1007/BF03355475
43. M.L. Saucedo-Muñoz, A. Ortiz-Mariscal, V.M. Lopez-Hirata, J.D. Villegas-Cardenas, A.M. Paniagua-Mercado, Microstructure characterization of aged heat resistant steels, in *147th annual meeting & exhibition supplemental proceedings*, vol. 76, ed. by The Minerals, Metals and Materials Society (Springer, Cham, 2018), pp. 803–810
44. V. Javaheri, F. Shahia, M. Mohammadnezhad, M. Tamizifar, M. Naseri, The effect of Nb and Ti on structure and mechanical properties of 12Ni-25Cr-0.4C austenitic heat-resistant steel after aging at 900 °C for 1000 h. J. Mater. Eng. Perform. **23**, 3558–3566 (2014)
45. De Cooman BC, Speer JG. Fundamentals of Steel Product Physical Metallurgy. AIST. 2011; Chapter 4, Austenite Descomposition in Fe-C-X Alloy Systems, pp. 135–191
46. M. McGrath, D. Van Aken, On the crystallography of peritectic austenite and the role of primary ferrite in high manganese and aluminum steels. Inter. J. Metalcast. **6**, 35–50 (2012). https://doi.org/10.1007/BF03355532